

ARTICLE

Open Access

# Laser-induced selective metallization of conductive patterns on silicone via copper carbonate hydroxide coating

Yuan Wei<sup>1✉</sup>, Xueqian Yang<sup>2</sup>, Haifeng Tian<sup>3</sup>, Ruoyan Miao<sup>2</sup>, Hai Tan<sup>3</sup>, Simon S. Park<sup>4</sup> and Xuewen Wang<sup>1,2✉</sup>

## Abstract

Flexible electronics demand stretchable, high-performance interconnects for wearable and implantable applications. However, conventional methods such as direct-ink writing or doped-activator metallization face challenges including thermal degradation risks from high-temperature sintering, complex multi-step chemical procedures with toxic precursors. Here, we introduce an updated laser-induced selective metallization (LISM) for fabricating stretchable copper electrodes directly on a commercial polysiloxane rubber. This approach employs a spray-coated copper carbonate hydroxide activator, followed by near-infrared laser activating. Laser irradiation leads to the reduction of copper ions, along with the formation of amorphous carbon domains and micro-nanoscale surface structures. Electroless copper plating (ECP) and electroplating (EP) are subsequently performed to form continuous, low-resistivity serpentine traces. Comprehensive characterization verifies the successful reduction of copper and the robust integration of the electrode into the substrate. Mechanical testing shows that the structure maintains its electrical performance under repeated cyclic deformation. Functional demonstrations including electrocardiogram (ECG) patch, LED arrays, and wireless antennas showcase practical applicability of the proposed approach. Additionally, LISM operates at ambient temperature without toxic precursors and it minimizes chemical consumption and provides exceptional durability. This method advances next-generation electronics requiring both mechanical flexibility and electrical reliability.

## Introduction

Flexible electronics are becoming increasingly important with rising demands for surface-conformable and mechanically tolerant devices<sup>1</sup>. These technologies establish the stretchable interconnect and sensing platform required for mechanically resilient, high-fidelity wearable devices<sup>2–5</sup>, flexible displays<sup>6–9</sup>, medical sensors<sup>10–12</sup> capable of maintaining electrical performance under mechanical deformations<sup>13,14</sup>. Consequently, the formation of reliable conductive patterns on elastomeric

substrates has become a central challenge in the development of stretchable electronic systems<sup>15</sup>.

Common elastomeric substrates include polydimethylsiloxane (PDMS) and commercial polysiloxane rubbers like Ecoflex<sup>TM</sup> provide high stretchability, low modulus, and biocompatibility. However, Ecoflex<sup>TM</sup>'s surface energy is low ( $14.17 \text{ mJ m}^{-2}$ )<sup>16</sup>, even below Teflon's ( $19.5 \text{ mJ m}^{-2}$ )<sup>17</sup>, hindering uniform deposition of metal films or conductive inks<sup>18</sup>. Although techniques like oxygen plasma, UV/ozone treatment, and silane primers can improve wettability, they introduce added complexity, require specialized equipment, may compromise substrate integrity, and tend to lose effectiveness over time. Direct printing of metal nanoparticle inks such as inkjet or aerosol-jet avoids lithographic masks, but they typically need thermal sintering above  $150^\circ\text{C}$ , risking substrate deformation or degradation<sup>19</sup>. Liquid metal is also utilized in combination with elastomeric substrates to fabricate

Correspondence: Yuan Wei (yuan.wei@nwafu.edu.cn) or Xuewen Wang (iamxwwang@nwpu.edu.cn)

<sup>1</sup>Institute of Future Agriculture (IFA), Northwest A&F University, Yangling, Shaanxi 712100, China

<sup>2</sup>Frontiers Science Center for Flexible Electronics, Xi'an Institute of Flexible Electronics (IFE) and Xi'an Institute of Biomedical Materials & Engineering, Northwestern Polytechnical University, Xi'an 710072, China

Full list of author information is available at the end of the article

© The Author(s) 2026



**Open Access** This article is licensed under a Creative Commons Attribution-NonCommercial-NoDerivatives 4.0 International License, which permits any non-commercial use, sharing, distribution and reproduction in any medium or format, as long as you give appropriate credit to the original author(s) and the source, provide a link to the Creative Commons licence, and indicate if you modified the licensed material. You do not have permission under this licence to share adapted material derived from this article or parts of it. The images or other third party material in this article are included in the article's Creative Commons licence, unless indicated otherwise in a credit line to the material. If material is not included in the article's Creative Commons licence and your intended use is not permitted by statutory regulation or exceeds the permitted use, you will need to obtain permission directly from the copyright holder. To view a copy of this licence, visit <http://creativecommons.org/licenses/by-nc-nd/4.0/>.

stretchable electronic electrodes. While these liquid metal systems exhibit impressive stretchability (>500%), they present several challenges. Due to their inherently high surface tension and propensity for oxidation, flexible electrodes based on liquid metal generally suffer from issues such as poor adhesion<sup>20,21</sup>, elevated resistivity<sup>22</sup>, and increased susceptibility to oxidation<sup>23,24</sup>.

While existing LISM techniques demonstrate feasibility as an alternative low-temperature method using activators, like Cr and Pd complexes (mixed with substrate material) and palladium or silver salts (wet-coating on the substrate surface), with electroless plating avoids thermal damage but involves activator-substrate composite preparing, generates waste and stress-prone delamination interfaces<sup>25–28</sup>, depends on expensive or toxic activators (e.g., Cr and Pd complexes<sup>29,30</sup>) and inadequately addresses long-term mechanical durability under repeated deformations<sup>31–39</sup>. An attempt using LISM on the Ecoflex<sup>TM</sup> is performed in 2022<sup>18</sup>, a conductive pattern is fabricated on a black flexible composite made of Ecoflex<sup>TM</sup> and Cu<sub>2</sub>Cr<sub>2</sub>O<sub>5</sub> powder through LISM process. However, most of the Cu<sub>2</sub>Cr<sub>2</sub>O<sub>5</sub> powder is not utilized. Instead, it transforms the Ecoflex<sup>TM</sup> from a transparent flexible material into pure black, resulting in a loss of some mechanical properties. Additionally, there is a potential risk of the Cu<sub>2</sub>Cr<sub>2</sub>O<sub>5</sub> powder contaminating both the environment and the human body. Further comparisons of flexible electrodes produced by other methods and LISM are presented in Supplementary Tables 1 and 2. In summary, the ideal flexible electronic substrate material—Ecoflex<sup>TM</sup>, urgently requires a method for electrode patterning that can ensure strong interface strength, be mask-free, non-toxic, and harmless in the process, and not alter the properties of the substrate material, while enabling rapid and free-form pattern formation. The objective of this study is to demonstrate the novel process that meets the mentioned requirements.

This study presents an innovative LISM approach, which offers a simple, mask-free, localized method to form freely designed metal patterns on pure polymers (not composites) at room temperature, utilizing spray-coated Cu<sub>2</sub>(OH)<sub>2</sub>CO<sub>3</sub> as a single-step, eco-friendly activator on untreated Ecoflex<sup>TM</sup>. Then, the NIR laser not only roughens the Ecoflex<sup>TM</sup> surface but also directly reduces Cu<sup>2+</sup> from Cu<sub>2</sub>(OH)<sub>2</sub>CO<sub>3</sub> into Cu<sup>0</sup> nanoparticles (confirmed by micro-area X-ray photoelectron spectroscopy Micro-XPS, time-of-flight secondary ion mass spectrometry ToF-SIMS), which serve as catalytic seeds for electroless copper plating (ECP). This direct laser seeding mechanism has not been demonstrated previously on pure silicone substrates. Furthermore, a sequence of ECP and electroplating (EP) produces dense, low-resistivity copper strongly adhered to an ultra-soft silicone. Notably, unreacted Cu<sub>2</sub>(OH)<sub>2</sub>CO<sub>3</sub> activation material can be quantitatively recovered and reutilized without performance degradation across multiple processing cycles, demonstrating the

approach's inherent sustainability and material efficiency (Supplementary Movie S1).

## Results and discussion

### Characterization of LISM process and mechanism of laser activation

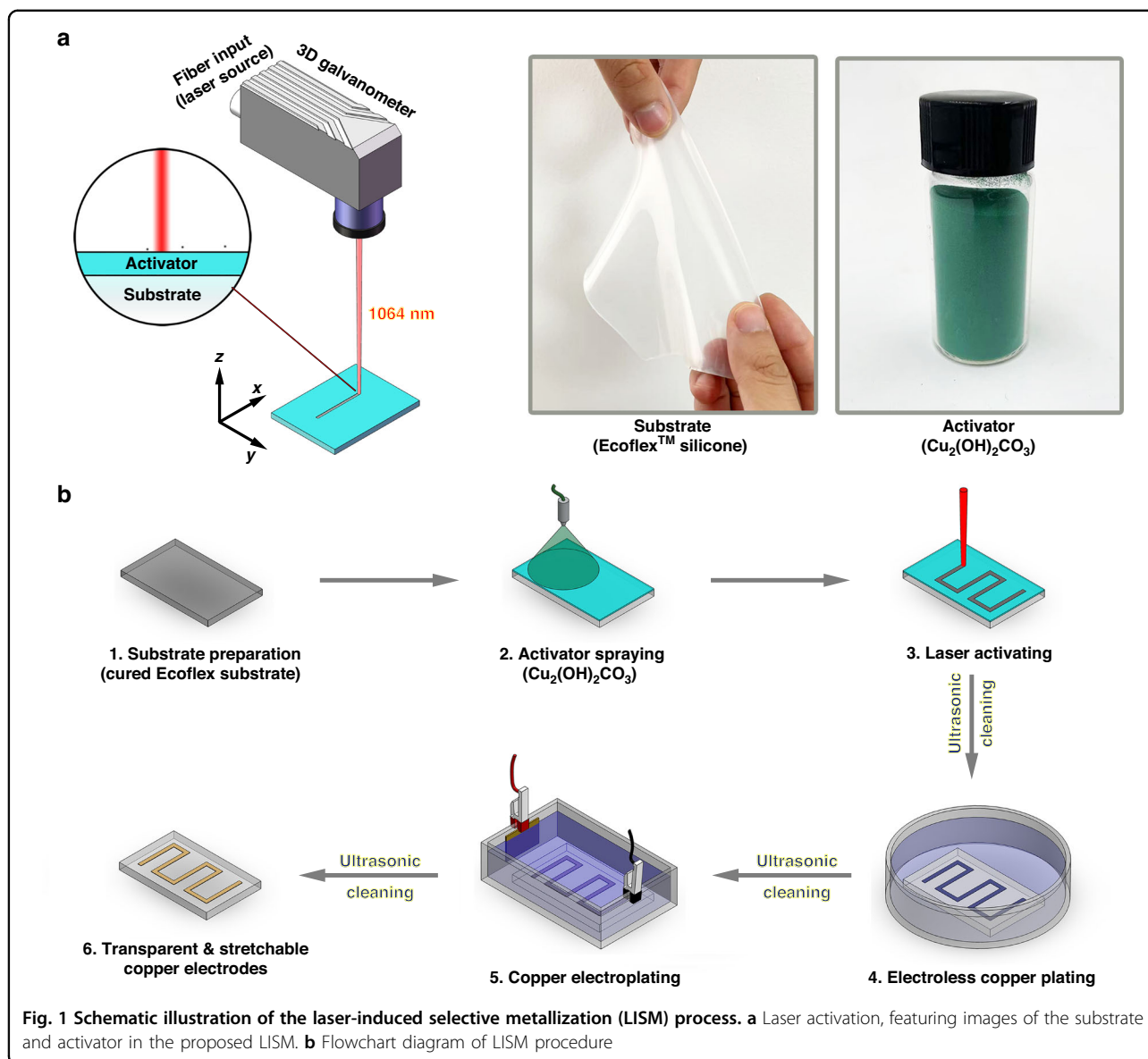
Figure 1 illustrates the proposed LISM process for creating a conductive pattern on the Ecoflex<sup>TM</sup> surface. This process consists of five main steps: substrate preparation, activator spraying, laser activation, ECP, and EP, as shown in Fig. 1b. Ecoflex<sup>TM</sup> 00-30 is selected as the substrate material due to its excellent stretchability, chemical stability, and biocompatibility.

The process begins with a pre-prepared Ecoflex<sup>TM</sup> 00-30 substrate, which receives a manually sprayed layer of commercial activator to ensure uniform coverage (see Supplementary Figs. S1 and S2). Next, a 1064 nm laser irradiates the activator layer using optimized settings determined from copper deposition quality tests (see Supplementary Fig. S3). Following this, the selective metallization process starts with ECP, where a commercial bath solution is used to deposit a continuous copper layer on the areas activated by the laser through autocatalytic reduction. To further improve the thickness and conductivity of the copper layer, the sample undergoes an EP process, resulting in a denser copper layer. With the modified activator and LISM process, the laser directly irradiates the activator layer instead of the combined layer of the substrate and activator. This necessitates a deeper understanding of the laser activation process.

Copper is chosen as the primary conductive material due to its low resistivity ( $1.7 \times 10^{-8} \Omega \text{ m}$ ) compared to nickel ( $6.9 \times 10^{-8} \Omega \text{ m}$ ). The ECP-EP sequence produced adherent traces with a resistivity of  $3.25 \times 10^{-8} \Omega \text{ m}$ —significantly lower than single-step ECP layers (typically  $> 10^{-7} \Omega \text{ m}$ <sup>29</sup>). In addition, copper creates less interfacial stress with Ecoflex<sup>TM</sup>, reducing the risk of delamination during deformation. While nickel may have advantages in terms of oxidation resistance, etc., selective nickel plating can be applied after ECP for other functions if needed.

Comparative analysis of the substrate surface profiles before and after laser activation reveals significant changes in surface roughness parameters. Specifically, the surface becomes noticeably rougher following laser activation. The variation of surface roughness ( $S_a$  and  $S_q$ ) with laser output energy is shown in Supplementary Fig. S4a, b. A more detailed view of the activated area is presented in Fig. 2e. Additionally, contact angle tests indicate that the surface after laser activation exhibits a higher contact angle, as shown in Supplementary Fig. S4c, d. This suggests improved hydrophobicity of the activated surface.

As shown in Fig. 2a, e, laser activation results in the ablation and alteration of material at the substrate's surface, leading to a rougher texture. This change in surface

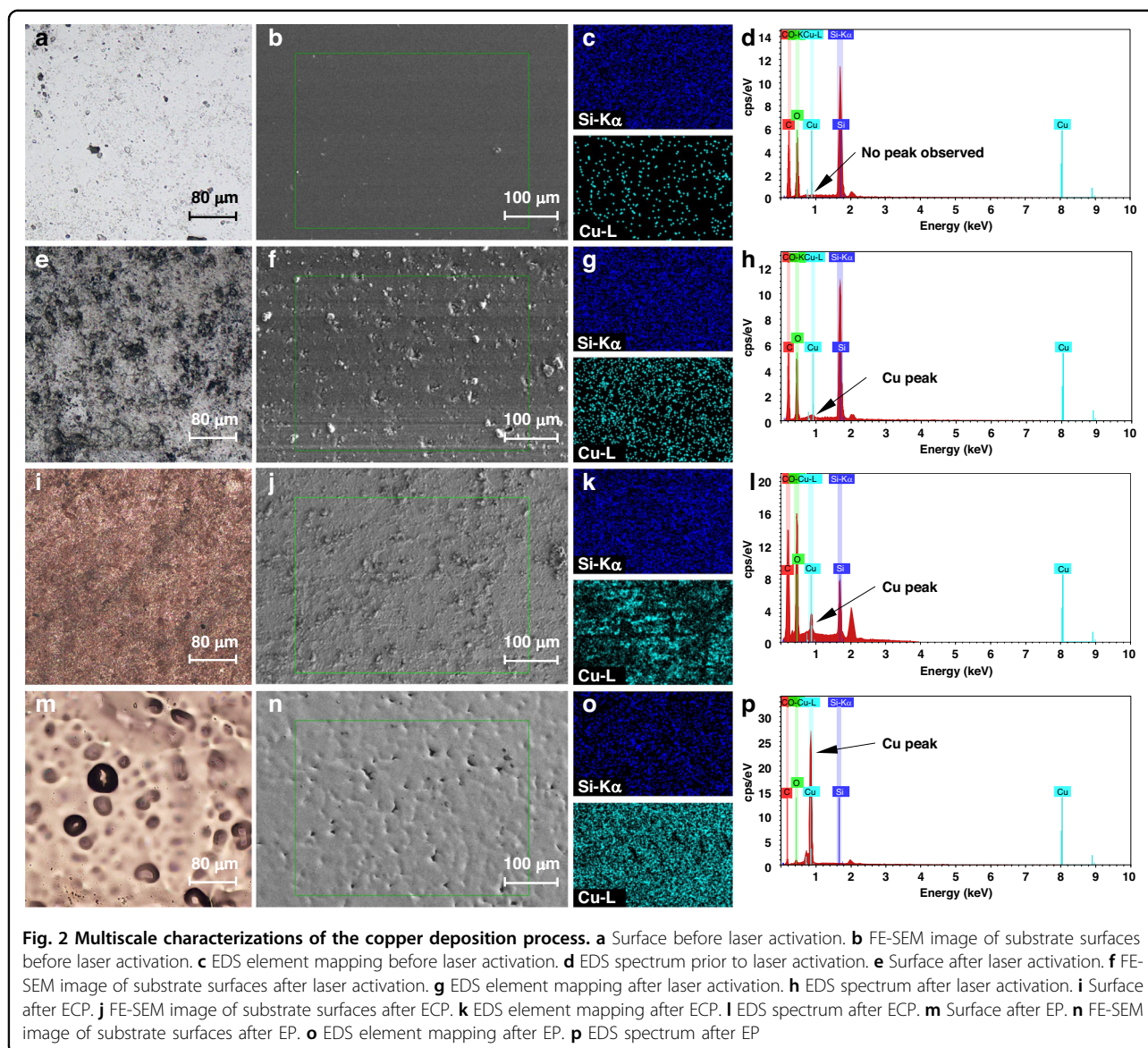


morphology enhances the substrate's ability to bond with subsequent coatings. After the ECP process, a thin copper layer forms on the laser-activated area, as illustrated in Fig. 2i. While this layer is electrically conductive, it has numerous microcracks and defects (see Supplementary Fig. S5), making it thin and fragile. Therefore, increasing its thickness is essential.

Figure 2m displays the surface after EP, where a thicker copper layer is evident. Although some defects remain, they do not significantly affect the electrochemical or mechanical properties of the copper layer. The fabrication process allows us to categorize the substrate surface into four distinct stages: before laser activation, after laser activation, after ECP, and after EP. The final thickness of

the copper layer, achieved at the end of the LISM process, is approximately  $32\ \mu\text{m}$  (see Supplementary Fig. S6).

To evaluate the bond strength between the copper layer and the substrate, a cross-cut test is conducted (Supplementary Fig. S7a, b). The test result, 5B indicates a strong interfacial bond at the copper-Ecoflex™ interface. Peel tests are also conducted, with results presented in Supplementary Fig. S7d. The peel strength between the copper trace and the substrate is measured at  $460\ \text{N/m}$ . For comparison, the peel strengths of two metal-based electrodes (Al-PVDF and Al-PU) with different binders are  $53\ \text{N/m}$  and  $72\ \text{N/m}$ , respectively<sup>40</sup>. The proposed LISM technique creates interlocking anchors within the Ecoflex™ substrate, ensuring a strong and reliable bond

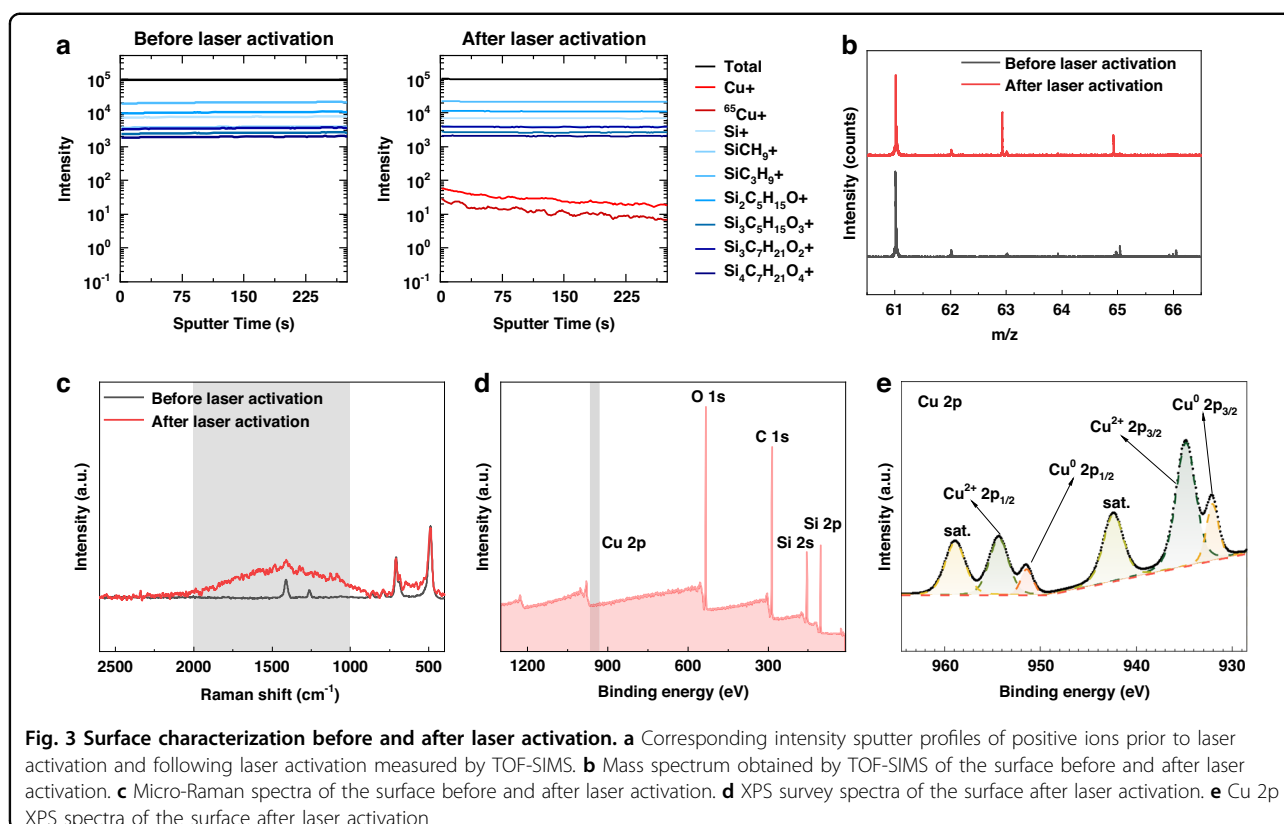


between the copper layer and the substrate. For the serpentine design of the copper trace, the enhanced interface strength significantly improves the electrode's stretchability and durability.

During the ECP and EP processes, copper is deposited in-situ on the rough surfaces, leading to the formation of strong bonds and connections with the textured substrate. The limits of pattern width and minimum spacing are approximately 160  $\mu\text{m}$  and 130  $\mu\text{m}$ , respectively, as shown in Supplementary Fig. S8. While the physical and chemical changes during the ECP and EP stages are well understood, it is crucial to investigate the changes occurring during the laser activation process. The substrate surfaces at various stages are examined using field emission scanning electron microscope (FE-SEM) and analyzed through energy-dispersive X-ray spectroscopy (EDS). Figure 2b, f, j, n presents FE-SEM

images of the substrate surface at four stages: before laser activation, after laser activation, after ECP, and after EP, respectively. Figure 2b serves as a reference for the substrate's surface, while Fig. 2f illustrates the rougher texture resulting from laser activation. Figure 2j, n shows the surface after ECP and EP, respectively. Figure 2c, g, k, o displays the corresponding EDS element mappings for silicon (Si) and copper (Cu) at each stage, covering the same area as the FE-SEM images. Additionally, Fig. 2d, h, l, p presents the EDS spectra for each stage.

Before laser activation, no significant copper distribution or Cu peak is observed, as shown in Fig. 2c, d. However, Fig. 2g indicates the presence of copper after laser activation, with a corresponding Cu peak in Fig. 2h. After ECP, Fig. 2k, l reveals increased copper deposition and a stronger Cu peak in both the element mapping and spectrum, confirming the



formation of a copper layer with numerous defects on the rough substrate surface, as seen in Fig. 2i, j. Finally, Fig. 2o presents the element mapping after EP, showing denser copper deposition and a significant reduction in the Si element, while Fig. 2p displays the spectrum after EP, confirming the successful deposition of a complete copper layer, as observed in the optical and SEM images shown in Fig. 2m, n.

The Time-of-Flight secondary ion mass spectrometer (TOF-SIMS, ION TOF Model 5-100) is used to analyze the elemental composition of the substrate surface, specifically focusing on the effect of laser activation. Figure 3a shows the intensity sputter profiles of positive ions before and after laser activation on the substrate surface. Notably,  $\text{Cu}^+$  and  $^{65}\text{Cu}^+$  ions are detected following the laser activation. Figure 3b presents the TOF-SIMS mass spectrum, where peaks at mass-to-charge ratios around 62.9 and 64.9 are observed after laser activation, confirming the presence of  $\text{Cu}^+$  and  $^{65}\text{Cu}^+$  ions.

Micro-XPS spectra are obtained to investigate the valence of the copper element. Figure 3d shows the XPS survey spectra corresponding to the surface after laser activation and Fig. 3e shows the high-resolution Cu 2p XPS spectrum. The result is fitted using a Lorentzian-Gaussian function, with fitting peaks depicted as dashed lines and the raw data as a dotted line. This fitting process allows for a more accurate analysis of the spectral peaks. The spectrum

reveals prominent  $\text{Cu} 2p_{1/2}$  and  $\text{Cu} 2p_{3/2}$  attributed to  $\text{Cu}^{2+}$  appear at 954.0 eV and 934.5 eV, respectively, along with the associated shake-up satellite peaks in the ranges of 957–963 eV and 938–945 eV. Notably, two peaks corresponding to  $\text{Cu}^0$  are observed, with  $\text{Cu} 2p_{1/2}$  and  $\text{Cu} 2p_{3/2}$  at 951.2 eV and 931.6 eV, respectively. The emergence of these  $\text{Cu}^0$  peaks suggests a reduction in the oxidation state of some copper atoms on the surface, which could have implications for the material's properties and reactivity. Raman spectroscopic analysis of substrate surface is also performed. The results of Raman spectroscopic analysis for the surface before and after laser activation are shown in Fig. 3c, a broad band from 1000–2000  $\text{cm}^{-1}$  is observed, which indicates the presence of amorphous carbon<sup>32</sup>.

In summary, FE-SEM imaging and EDS analysis show the presence of Cu on the substrate surface following the laser activation process. TOF-SIMS results further confirm the existence of Cu after laser activation. Additionally, Micro-XPS analysis indicates the presence of both  $\text{Cu}^{2+}$  and  $\text{Cu}^0$  on the laser-activated surface.

Based on Raman spectroscopy results, a potential laser activation mechanism is proposed. The activator,  $\text{Cu}_2(\text{OH})_2\text{CO}_3$ , absorbs the laser and generates high temperatures, causing ablation, gasification, and carbonization of the Ecoflex<sup>TM</sup> substrate surface. This results in the formation of a rough surface and amorphous carbon. Concurrently, part of the  $\text{Cu}^{2+}$  is reduced to  $\text{Cu}^0$  due to

laser irradiation. The  $\text{Cu}^0$  acts as the seed for the ECP process, with activation completing upon the reduction of  $\text{Cu}^{2+}$  to  $\text{Cu}^0$ . This hypothesis is consistent with previous studies in the LISM literature<sup>29,41</sup>, which indicate that laser activation transforms the activator into metallic species. These metallic species then serve as active centers to initiate the ECP<sup>42</sup>. In addition, tests with other potential activators are performed, including Multi-Walled Carbon Nanotubes (MWCNT), basic copper phosphate and stannic oxide (Supplementary Fig. S9).

### Performance of silicone flexible electrodes

Electromechanical testing of LISM-fabricated electrodes employs serpentine copper traces with three distinct turn geometries: V-curved, U-curved, and S-curved (refer to Fig. 4a–c). During tensile elongation to failure, resistance is monitored simultaneously, revealing that fractures consistently occur at the stress-concentrated turnarounds. Notably, the copper-Ecoflex<sup>TM</sup> interface demonstrates no signs of delamination, which confirms the effectiveness of the laser-induced micro-roughened interlocking.

Furthermore, Fig. 4d, e demonstrates the average maximum strain and resistance for V-curved, U-curved, and S-curved samples. The V-curved electrodes achieve a maximum strain of 125% (see Fig. 4d), a significant enhancement made possible by the serpentine design and the LISM process. This improvement stands in contrast to the inherent ductility of copper, which typically fractures at strains below 5%<sup>43</sup>. During the stretching process, the change in resistance for all three types of samples remains minimal until complete rupture, as shown in Fig. 4f. Electrical stability is quantified during cyclic tensile fatigue testing (30% strain, 1083 cycles) on V-curved samples. Before 1050 cycles, the resistance fluctuates around 2%, but in the last few cycles, it increases sharply until fracture (Fig. 4g). Figure 4h illustrates the resistance of unencapsulated samples as a function of time when exposed to open air, the resistance increases rapidly initially, then stabilizes. The results of bending and twisting tests for electrical stability are shown in Supplementary Fig. S10. This observation highlights the ability of the LISM-fabricated electrodes to effectively handle mechanical stress, suggesting their suitability for applications that require flexibility and durability.

The resistivity  $\rho$  of LISM-fabricated traces is calculated using Eq. 1 as follows:

$$\rho = R \times \frac{A}{L} \quad (1)$$

where  $R$  is the resistance,  $A$  is the cross-sectional area of the circuit trace and  $L$  is the length of the circuit trace. The measured average resistivity of the circuit trace is  $3.25 \times 10^{-8} \Omega \text{ m}$ , while not reaching the resistivity of pure copper ( $1.7 \times 10^{-8} \Omega \text{ m}$ ), is significantly lower than that of

conductive traces made from  $\text{LaNiO}_3$ <sup>44</sup>, liquid metal Galinstan<sup>45</sup>, EGaln<sup>22</sup>, silver nanowire Ag NW<sup>46</sup>, and Ag NW with Au thin film<sup>47</sup>, as illustrated in Fig. 4i. Further tests to evaluate the durability of silicone flexible electrodes, including strain sweep tests, thermal aging, and sweat corrosion, are presented in Supplementary Figs. S12 and S13.

### Application of silicone flexible electrodes

The flexible and stretchable electrodes produced through the LISM process have a wide range of applications, including electrocardiogram (ECG) patches, LED lights, and antennas. Using the LISM procedure, an ECG patch is designed and fabricated with a conductive pattern on a round, transparent Ecoflex<sup>TM</sup> film. A central through-hole via allows copper traces to pass through and connect to soldering pads on the opposite side, facilitating interlayer connections without introducing soldering-induced stress. This patch works in conjunction with the customized ECG data acquisition device to create a three-lead ECG monitoring system, operating at a sampling rate of 0.32 kHz. As illustrated in Fig. 5a, b, when applied to specific locations on the torso of a 26-year-old healthy male, the Cu/Ecoflex<sup>TM</sup> ECG patch adheres closely to the skin, minimizing foreign body sensation and discomfort. Figure 5c displays the ECG signals obtained over a 30-minutes period, with a detailed analysis of a single pulse revealing excellent signal integrity that allows for clear distinction of characteristic waveforms, including the P wave, R wave, and S wave. The direct fabrication of the patch on biocompatible Ecoflex<sup>TM</sup> proves advantageous, as it eliminates the need for interfacial adhesives that can degrade signal quality. Additionally, Fig. 5d shows the comparison of ECG signals obtained under two conditions “Resting” and “Slow walking”. As a result of motion, the signal exhibits slight baseline drift and noise, but the overall integrity remains good, and the ECG signal with good quality can still be reconstructed through simple filtering. It suggests that the patch could provide an option for collecting ECG signals during mild skin deformation (<10% strain) associated with normal movement, demonstrating exceptional comfort, skin compatibility, and effective signal collection. A further comparison between the proposed ECG monitoring system and a commercial ECG monitoring system is shown in Supplementary Fig. S11.

Furthermore, a silicone circuit featuring curved traces and nine blue LEDs is designed and fabricated using the proposed LISM, as shown in Supplementary Fig. S14a. The LEDs are soldered in parallel on the circuit and the serpentine circuit sustains up to 30% bending and stretching without any dimming of the LEDs (Supplementary Movie S2), highlighting its stability under dynamic deformation. In addition to ECG patches and LED circuits, the LISM method enables the fabrication of various flexible electronic devices tailored to different application scenarios, such as flexible antennas. Supplementary Fig. S14b–d and Supplementary Movie S3

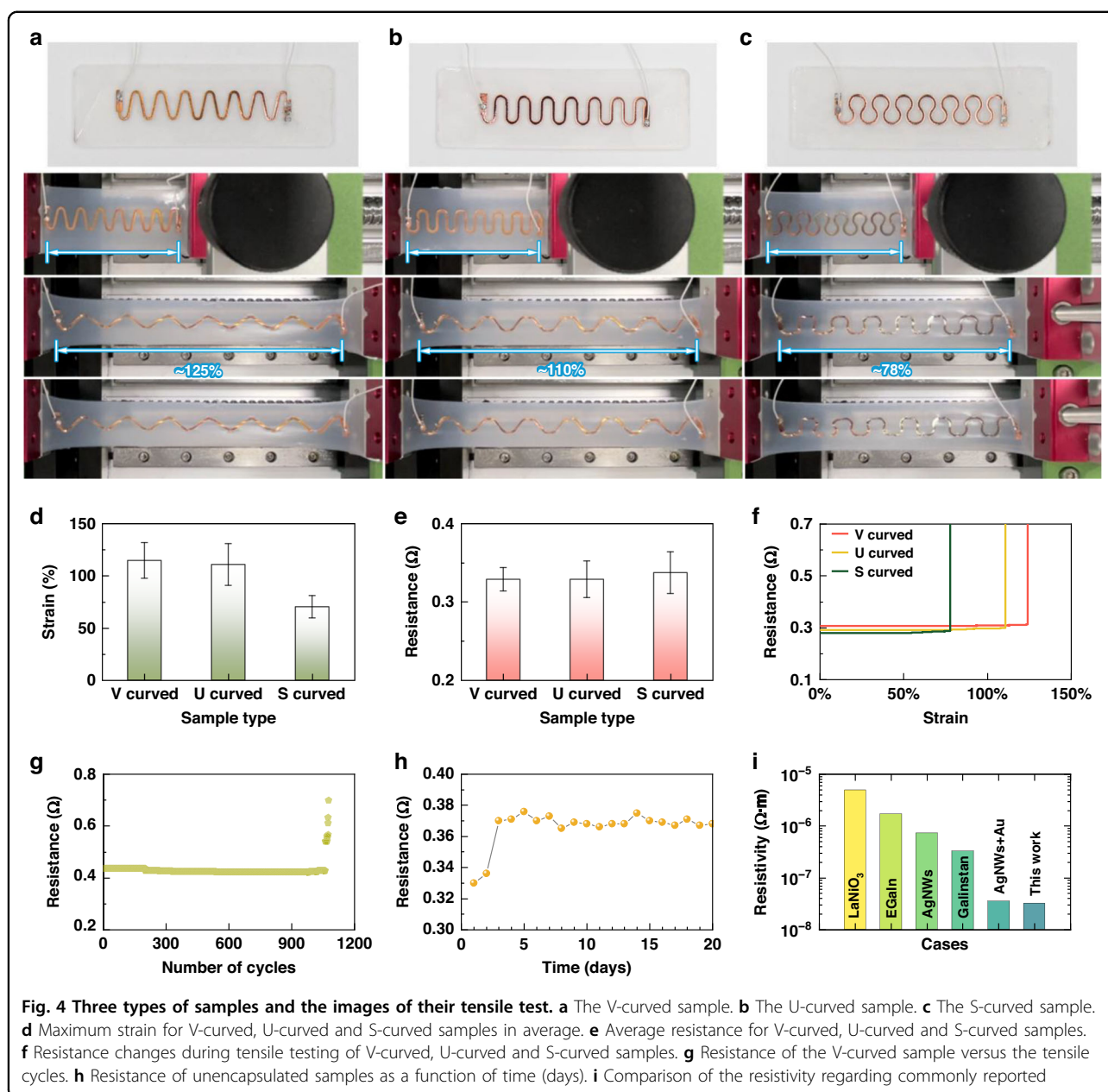
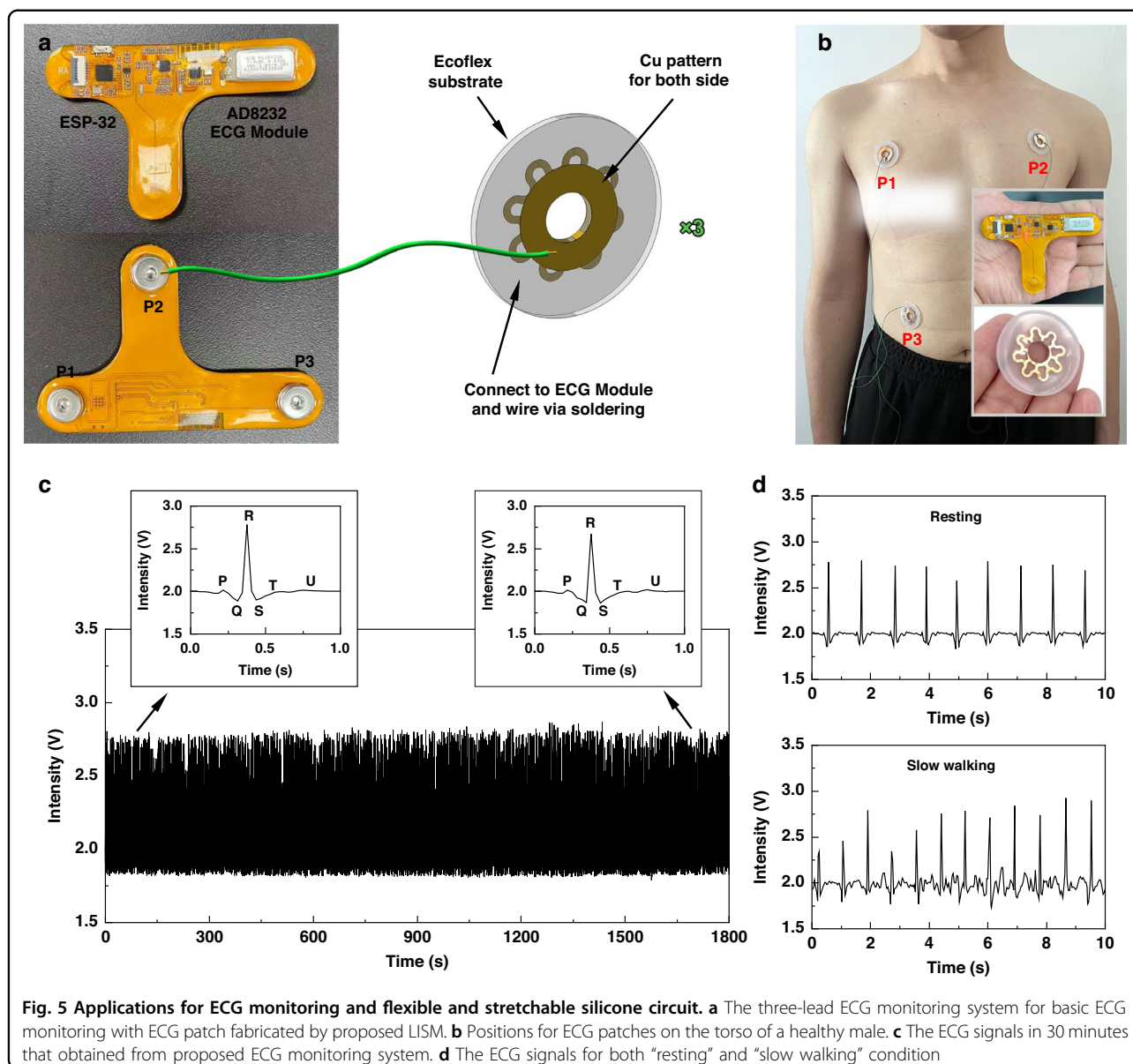


**Fig. 4** Three types of samples and the images of their tensile test. **a** The V-curved sample. **b** The U-curved sample. **c** The S-curved sample. **d** Maximum strain for V-curved, U-curved and S-curved samples in average. **e** Average resistance for V-curved, U-curved and S-curved samples. **f** Resistance changes during tensile testing of V-curved, U-curved and S-curved samples. **g** Resistance of the V-curved sample versus the tensile cycles. **h** Resistance of unencapsulated samples as a function of time (days). **i** Comparison of the resistivity regarding commonly reported

characterize a bendable wireless-charging antenna. The two antennas, functioning as the transmitting and receiving ends, can be simultaneously attached to the surface of a cylinder to transmit electrical energy. In Supplementary Movie S3, two bending conditions are shown for both transmitting and receiving ends: one with the antennas bent in the same direction (transmitting antenna curvature radius: 30 mm, receiving antenna curvature radius: 40 mm), and the other with the antennas bent in opposite directions (curvature radius of both antennas: 50 mm). This flexibility highlights the potential of LISM in advancing flexible electronics across various applications.

In reported studies, completing the LISM process typically only involved ECP. However, in our proposed LISM process, an EP step is added after ECP. This modification is necessary because the copper layer obtained through ECP alone did not exhibit optimal electrical and mechanical properties. Microscopic observations reveal numerous cracks, and the resistance is relatively high. While attempts to extend the ECP time exhibit some improvement, they also increase the risk of coating degradation, including the attachment of free-floating copper particles to the copper layer's surface. Therefore, we introduce the EP process, which resulted in a copper layer with improved thickness and enhanced



electrical and mechanical properties. The difference in performance of the copper layer after ECP regarding the present study and other reported studies may be attributed to the differences in the usage method of the activator. In comparison to the mixed activator combined with the base material, the activator coating that consists solely of the activator on the surface results in a lower nucleation density for copper crystallization following the laser activation process. This reduced nucleation density leads to a less compact copper layer being deposited on the activated surface<sup>48</sup>.

## Conclusions and outlook

We demonstrate an updated LISM for fabricating flexible and stretchable copper electrodes directly onto Ecoflex<sup>TM</sup> substrates. An eco-friendly  $\text{Cu}_2(\text{OH})_2\text{CO}_3$  spray-coating is

converted via laser processing to create micro-roughened carbonaceous surfaces and catalytic  $\text{Cu}^0$  sites. Subsequent ECP/EP produces highly conductive copper traces ( $\approx 3.25 \times 10^{-8} \Omega \text{ m}$ ) mechanically interlocked at the substrate interface, achieving 460 N/m peel strength and 5B adhesion. This architecture enables minimal resistance drift (<2.0%) under strain and sustains performance through 1000 stretch-release cycles at 30% strain. Serpentine designs attain 125% strain tolerance via geometric optimization rather than intrinsic copper ductility. Functional applications—including ECG patches with high-fidelity and skin conformality, stretchable/foldable LED arrays, and a wireless antenna—operate stably during deformation without toxic precursors or thermal sintering. While advancing the fabrication of flexible electrodes with an emphasis on simplicity and

sustainability, future work will concentrate on several key areas. First, efforts will be directed toward addressing copper's susceptibility to oxidation by developing oxidation-resistant coatings or conformal encapsulation strategies. Additionally, although we have a preliminary understanding that the proposed method can be roughly applied to PDMS, thermoplastic polyurethane (TPU), and polyimide (PI), the research will evaluate environmental stability for wearable applications, expanding the range of substrate materials. Finally, the study aims to scale the fabrication process for complex multi-layer circuits while integrating additional functional materials, thereby enhancing the overall performance and versatility of the electrodes.

## Experimental section

### Fabrication of activator-coated Ecoflex™ substrates

Ecoflex™ 00-30 platinum-cure silicone rubber (Smooth-On Inc.) serves as the substrate. Part A and Part B are mixed following manufacturer instructions, poured into an aluminum mold, and cured 24 h to form soft, stretchable films with a minimum 0.4 mm thickness. Copper carbonate hydroxide ( $\text{Cu}_2(\text{OH})_2\text{CO}_3$ , particle size 30–50  $\mu\text{m}$ ; Shanghai Macklin Biochemical Technology Co., Ltd) is applied as an activator via a commercial powder spraying system, achieving a controlled dosage of 11.5 mg/cm<sup>2</sup>.

### Laser-activated metallization

The activator layer is selectively irradiated using a pulsed near-infrared (NIR) laser scanning system (LRDB-FIB30, Xi'an Langrui) with a wavelength of 1064 nm, spot size of 50  $\mu\text{m}$ , pulse duration of 20 ns, and adjustable power (0–30 W). Optimized parameters include a laser frequency of 40 kHz, output power of 10 W, and scanning speed of 1200 mm/s. After irradiation, ultrasonic cleaning then removes residual activator for reuse, the detailed process of reusing activator is shown in Supplementary Movie S1.

### Selective metallization process

Following the laser activation, the substrate undergoes ECP using a commercial solution (Q/YS.118 A/B; Guangzhou Yi Shun Chemical Co., Ltd) at 45 °C and pH of 12.8 for 20 minutes. This process deposits a thin copper layer (approximately 21.3  $\mu\text{m}$ ) on irradiated regions. To enhance thickness, EP is performed using solution Q/YS.138 at room temperature. A copper anode and the sample (cathode) are subjected to a constant current of 0.2 A for 20 minutes and the copper layer reaches 31.3  $\mu\text{m}$  thickness. The thickness of the copper layer is measured by Bruker Dektak XT step profilometry. Final ultrasonic cleaning eliminates residual processing compounds.

### Characterization of interfacial properties, mechanical and electrical properties

Characterization of the substrate surface at different stages is performed by scanning electron microscopy surface imaging (SEM, ZEISS Gemini SEM 300), energy-dispersive X-ray spectroscopy (EDS, ZEISS Gemini SEM 300), Raman spectroscopy (Renishaw-inVia, 785 nm laser), and Micro-XPS (Thermo Fisher K-Alpha). The interfacial adhesion strength between copper traces and Ecoflex™ is quantified via cross-cut tests (ASTM D3359-23 Method B) and peel tests, yielding an average peel strength of 460 N/m. Uniaxial tensile tests employ a custom ZSL-1200 mechanical testing platform (Yangling Zishi Electronic Technology Co.), stretching samples at 10 mm/min while monitoring resistance in real time. For cyclic durability, S-curved traces underwent 1000 stretching cycles at 30% strain. Electrical resistivity is measured using a Keithley DMM6500 6.5-digit multimeter.

### Application devices manufacturing

ECG patches utilize proposed LISM to generate conductive patterns on 1.5 mm thick circular Ecoflex™ films with central through-holes for vertical interconnects. AWG 30 wires are soldered to copper traces, interfacing with AD8232 ECG signal conditioning modules and ESP-32 microcontrollers. Three-lead systems acquire signals from human subjects (26-year-old male tested at 0.32 kHz sampling). LED arrays and wireless antennas—soldered onto LISM-patterned circuitry—maintain functionality under mechanical deformations.

### Author details

<sup>1</sup>Institute of Future Agriculture (IFA), Northwest A&F University, Yangling, Shaanxi 712100, China. <sup>2</sup>Frontiers Science Center for Flexible Electronics, Xi'an Institute of Flexible Electronics (IFE) and Xi'an Institute of Biomedical Materials & Engineering, Northwestern Polytechnical University, Xi'an 710072, China. <sup>3</sup>College of Mechanical and Electronic Engineering, Northwest A&F University, Yangling, Shaanxi 712100, China. <sup>4</sup>College of Engineering & Computer Science, VinUniversity, Gia Lâm, Hanoi 100000, Vietnam

### Author contributions

Y.W. and X.W.: Conceptualization, writing, and reviewing. Y.W., X.Y., H.T., and R.M.: Methodology, investigation, writing original manuscript, writing and reviewing, performing all experiments. Y.W., H.T., and S.P.: Project administration, resources; S.P., and X.W.: Performing partial experiments.

### Data availability

All data supporting this study are available within the manuscript and supplementary materials. Additional datasets are obtainable from the corresponding author upon reasonable request.

### Conflict of interest

The authors declare no competing interests.

**Supplementary information** The online version contains supplementary material available at <https://doi.org/10.1038/s41378-026-01207-2>.

Received: 6 August 2025 Revised: 30 November 2025 Accepted: 26 December 2025  
Published online: 16 March 2026

## References

- Huang, W. Polymers for flexible electronics. *Chin. J. Polym. Sci.* **40**, 1513–1514 (2022).
- Jeerapan, I., Sangsudcha, W. & Phokhonwong, P. Wearable energy devices on mask-based printed electrodes for self-powered glucose biosensors. *Sens. Bio Sens. Res.* **38**, 100525 (2022).
- Wang, M. et al. A wearable electrochemical biosensor for the monitoring of metabolites and nutrients. *Nat. Biomed. Eng.* **6**, 1225–1235 (2022).
- Nyein, H. Y. Y. et al. A wearable patch for continuous analysis of thermo-regulatory sweat at rest. *Nat. Commun.* **12**, 1823 (2021).
- Yang, Y. et al. A laser-engraved wearable sensor for sensitive detection of uric acid and tyrosine in sweat. *Nat. Biotechnol.* **38**, 217–224 (2020).
- Choi, D. K. et al. Highly efficient, heat dissipating, stretchable organic light-emitting diodes based on a MoO<sub>3</sub>/Au/MoO<sub>3</sub> electrode with encapsulation. *Nat. Commun.* **12**, 2864 (2021).
- Nam, M. et al. Highly reliable and stretchable OLEDs based on facile patterning method: toward stretchable organic optoelectronic devices. *npj Flex. Electron* **8**, 17 (2024).
- Shi, X. et al. Large-area display textiles integrated with functional systems. *Nature* **591**, 240–245 (2021).
- Choi, H. W. et al. Smart textile lighting/display system with multifunctional fibre devices for large scale smart home and IoT applications. *Nat. Commun.* **13**, 814 (2022).
- Xu, Q. et al. Highly flexible, high-performance, and stretchable piezoelectric sensor based on a hierarchical droplet-shaped ceramics with enhanced damage tolerance. *Adv. Mater.* **36**, 2311624 (2024).
- Chen, L. et al. Wearable sensors for breath monitoring based on water-based hexagonal boron nitride inks made with supramolecular functionalization. *Adv. Mater.* **36**, 2312621 (2024).
- Meng, K. et al. Wearable pressure sensors for pulse wave monitoring. *Adv. Mater.* **34**, 2109357 (2022).
- Lan, T. et al. Treefrog-inspired flexible electrode with high permeability, stable adhesion, and robust durability. *Adv. Mater.* **36**, 2404761 (2024).
- Kim, J. J. et al. Tri-system integration in metal-oxide nanocomposites via in-situ solution-processed method for ultrathin flexible transparent electrodes. *Nat. Commun.* **15**, 2070 (2024).
- Zhang, H. et al. Recent advances in nanofiber-based flexible transparent electrodes. *Int. J. Extrem. Manuf.* **5**, 32005 (2023).
- Wang, S.-J. et al. MXene reinforced organohydrogels with ultra-stability, high sensitivity and anti-freezing ability for flexible strain sensors. *J. Mater. Chem. C* **10**, 11914–11923 (2022).
- He, C., Mighri, F., Guiver, M. D. & Kaliaguine, S. Sorption of water/methanol on teflon and hydrocarbon proton exchange membranes. *ACS Appl. Mater. Interfaces* **8**, 12541–12551 (2016).
- Yoo, B., Bowen, D., Lazarus, N. & Pines, D. Laser direct structured 3D circuits on silicone. *ACS Appl. Mater. Interfaces* **14**, 18854–18865 (2022).
- Khan, Y. et al. A new frontier of printed electronics: flexible hybrid electronics. *Adv. Mater.* **32**, 1905279 (2020).
- Ma, J. et al. Shaping a soft future: patterning liquid metals. *Adv. Mater.* **35**, 2205196 (2023).
- Hu, L., Wang, L., Ding, Y., Zhan, S. & Liu, J. Manipulation of liquid metals on a graphite surface. *Adv. Mater.* **28**, 9210–9217 (2016).
- Kim, M. et al. Nanowire-assisted freestanding liquid metal thin-film patterns for highly stretchable electrodes on 3D surfaces. *npj Flex. Electron* **6**, 99 (2022).
- Creighton, M. A. et al. Oxidation of gallium-based liquid metal alloys by water. *Langmuir* **36**, 12933–12941 (2020).
- Kim, M., Lim, H. & Ko, S. H. Liquid metal patterning and unique properties for next-generation soft electronics. *Adv. Sci.* **10**, 2205795 (2023).
- Kordas, K. et al. Laser-induced surface activation of LTCC materials for chemical metallization. *IEEE Trans. Adv. Packag.* **28**, 259–263 (2005).
- Gerges, T., Semet, V., Lombard, P., Allard, B. & Cabrera, M. Rapid 3D-plastronics prototyping by selective metallization of 3D printed parts. *Addit. Manuf.* **73**, 103673 (2023).
- Xiang, H., Zhou, Z., Yang, Y., Yu, Z. & Liu, J. Fabrication of metallic patterns on ordinary polymer substrates by laser direct activation and electroless plating. *Surf. Interfaces* **33**, 102209 (2022).
- Yu, F., Xu, H. & Zhou, T. Laser-induced selective metallization of epoxy resin: preparing ultra-thin and ultra-light motors. *Compos. Part A* **177**, 107946 (2024).
- Zhang, J., Zhou, T. & Wen, L. Selective metallization induced by laser activation: fabricating metallized patterns on polymer via metal oxide composite. *ACS Appl. Mater. Interfaces* **9**, 8996–9005 (2017).
- You, J.-L. et al. Electroless plating of a 5G copper antenna on polyimide patterned with laser-induced selective activation and curing of metal-organic catalyst. *Appl. Surf. Sci.* **599**, 153990 (2022).
- Liu, F. et al. Selective metallization on additive manufactured polymer for fabrication of integrated device. *J. Mater. Sci.* **57**, 1506–1515 (2022).
- Zhang, J., Zhou, T., Wen, L. & Zhang, A. Fabricating metallic circuit patterns on polymer substrates through laser and selective metallization. *ACS Appl. Mater. Interfaces* **8**, 33999–34007 (2016).
- Seiler, M., Gruben, J., Knauff, A., Barz, A. & Bliedtner, J. Laser beam activation of polymer surfaces for selective chemical metallization. *Procedia CIRP* **94**, 891–894 (2020).
- Yang, J., Cho, J. H. & Yoo, M. J. Selective metallization on copper aluminate composite via laser direct structuring technology. *Compos. Part B* **110**, 361–367 (2017).
- Wang, P. et al. Enabling 3D multilayer electronics through the hybrid of vat photopolymerization and laser-activated selective metallization. *Addit. Manuf.* **74**, 103717 (2023).
- Zhang, J., Zhou, T., Wen, L., Zhao, J. & Zhang, A. A simple way to achieve legible and local controllable patterning for polymers based on a near-infrared pulsed laser. *ACS Appl. Mater. Interfaces* **8**, 1977–1983 (2016).
- Xu, H. et al. Autocatalytic laser activator for both UV and NIR lasers: preparation of circuits on polymer substrates by selective metallization. *ACS Appl. Mater. Interfaces* **14**, 31411–31423 (2022).
- Lee, D. et al. Photocurable three-dimensional printing resin to enable laser-assisted selective electroless metallization for customized electronics. *ACS Appl. Polym. Mater.* **3**, 4735–4745 (2021).
- Xiang, H. et al. Selective metallization on ordinary polymer substrates by laser direct activation of copper phosphate or nickel phosphate. *Langmuir* **39**, 2063–2072 (2023).
- Park, G., Park, Y., Park, J. & Lee, J. Flexible and wrinkle-free electrode fabricated with polyurethane binder for lithium-ion batteries. *RSC Adv.* **7**, 16244–16252 (2017).
- Xiao, C., Feng, J., Xu, H., Xu, R. & Zhou, T. Scalable strategy to directly prepare 2D and 3D liquid metal circuits based on laser-induced selective metallization. *ACS Appl. Mater. Interfaces* **14**, 20000–20013 (2022).
- Xu, H., Feng, J., Yu, F., Huang, J. & Zhou, T. Laser-induced selective metallization on polymers for both NIR and UV lasers: preparing 2D and 3D circuits. *Ind. Eng. Chem. Res.* **62**, 395–404 (2023).
- Lazarus, N., Meyer, C. D. & Bedair, S. S. Stretchable inductor design. *IEEE Trans. Electron Devices* **62**, 2270–2277 (2015).
- Zhang, S. et al. Flexible LaNiO<sub>3</sub> film with both high electrical conductivity and mechanical robustness. *Ceram. Int.* **50**, 39830–39836 (2024).
- Zhao, Z., Soni, S., Lee, T., Nijhuis, C. A. & Xiang, D. Smart eutectic gallium-indium: from properties to applications. *Adv. Mater.* **35**, 2203391 (2023).
- Zhang, H. et al. Stretchable electrodes with interfacial percolation network. *Adv. Mater.* **36**, 2401550 (2024).
- Bang, J. et al. Stretchable and directly patternable double-layer structure electrodes with complete coverage. *ACS Nano* **16**, 12134–12144 (2022).
- Li, S. et al. Ultra-flexible stretchable liquid metal circuits with antimicrobial properties through selective laser activation for health monitoring. *Chem. Eng. J.* **482**, 149173 (2024).